**THE EUROPEAN
PHYSICAL JOURNAL C**

The reheating constraints to natural inflation in Horndeski gravity

Chen-Hsu Chien[1,a], **Seoktae Koh**[2,b], **Gansukh Tumurtushaa**[2,c]

[1] Leung Center for Cosmology and Particle Astrophysics, National Taiwan University, Taipei 10617, Taiwan, ROC
[2] Department of Science Education, Jeju National University, Jeju 63243, Korea

Abstract For the subclass of Horndeski theory of gravity, we investigate the effects of reheating on the predictions of natural inflation. In the presence of derivative self-interaction of a scalar field and its kinetic coupling to the Einstein tensor, the gravitational friction to inflaton dynamics is enhanced during inflation. As a result, the tensor-to-scalar ratio r is suppressed. We place the observational constraints on a natural inflation model and show that the model is now consistent with the observational data for some plausible range of the model parameter Δ, mainly due to the suppressed tensor-to-scalar ratio. To be consistent with the data at the 1σ (68% confidence) level, a slightly longer natural inflation with $N_k \gtrsim 60$ e-folds, longer than usually assumed, is preferred. Since the duration of inflation, for any specific inflaton potential, is linked to reheating parameters, including the duration N_{re}, temperature T_{re}, and equation-of-state ω_{re} parameter during reheating, we imposed the effects of reheating to the inflationary predictions to put further constraints. The results show that reheating consideration impacts the duration of inflation N_k. If reheating occurs instantaneously for which $N_{re} = 0$ and $\omega_{re} = 1/3$, the duration of natural inflation is about $N_k \simeq 57$ e-folds, where the exact value is less sensitive to the model parameter Δ compatible with the CMB data. The duration of natural inflation is longer (or shorter) than $N_k \simeq 57$ e-folds for the equation of state larger (or smaller) than 1/3 hence $N_{re} \neq 0$. The maximum temperature at the end of reheating is $T_{re}^{\max} \simeq 3 \times 10^{15}$ GeV, which corresponds to the instantaneous reheating. The low reheating temperature, as low as a few MeV, is also possible when ω_{re} is closer to 1/3.

1 Introduction

Cosmic inflation is a period of accelerated expansion of the early universe and an attractive mechanism for explaining the observed structures in the universe. It provides a solution to several puzzles, so-called cosmological problems, including the horizon, flatness, and monopole problems [1–5]. Current observations favor the inflationary paradigm for its prediction of an almost scale-invariant spectrum of primordial curvature perturbations imprinted in the cosmic microwave background (CMB) radiation and the large scale structure formations data [6–9]. The simplest model of inflation describes the period of exponential expansion of the early universe being driven by the slow-roll of a single scalar field known as the *inflaton*. To match the CMB temperature anisotropy measurements and give rise to a sufficient amount of inflation, the models of inflation share the flatness of the inflaton potential as a common feature among them [10,11]. This nontrivial requirement of flatness of inflaton potential creates fine-tuning problems, in particular, quantum corrections in the absence of a symmetry generically spoil the flatness of the potential, which is known as the η-problem.

In particle physics model of inflation, the flatness of the potential should be protected against radiative corrections that can arise from the inflaton self-interactions or from its coupling to matter fields, responsible for reheating the universe after inflation [12–14]. To protect the flatness of the inflaton potential against the radiative corrections, the symmetries of a system play an important role – e.g., as for the standard model Higgs field, supersymmetry can provide a natural protection against the radiative corrections [13,14]. If the inflaton is a pseudo-scalar axion, the axionic (shift) symmetry, $\phi \rightarrow \phi +$ constant, is another possible symmetry that protects the flatness of the inflaton potential. In this case, the inflaton potential arises from the breaking of a (global) shift symmetry, and the couplings of inflaton to matter fields do not affect the inflaton potential as long as the shift symmetry is respected. This mechanism was originally pro-

[a] e-mail: chenhsu0223@gmail.com

[b] e-mail: kundol.koh@jejunu.ac.kr

[c] e-mail: gansuh.mgl@gmail.com (corresponding author)

posed in Ref. [12] as *natural inflation*, and its implications in light of the observational data, as well as implementations in the other theories, have been discussed in Refs. [12–25]. In the natural inflation model, a rolling inflaton has a flat potential due to shift symmetries. Whenever a global symmetry is spontaneously broken, Nambu Goldstone bosons arise, with a potential that is exactly flat. However, the inflaton cannot roll and drive inflation if the shift symmetry is exact. Thus, to drive inflation, there must be additional explicit symmetry breaking hence these particles become pseudo-Nambu Goldstone bosons, with "nearly" flat potentials exactly as required by inflation [16]. The resulting inflaton potential is generally of the form $V(\phi) = \Lambda^4[1 + \cos(\phi/f)]$, where f is called the decay constant and is constrained by the observational data [12,15,16]. Despite its well established theoretical motivation and a simple form of the potential, the natural inflation model is disfavored at greater than 95% confidence by the observational data [10,11,26,27], especially after the recent announcement of the improved Planck + BICEP/Keck 2018 data [28]. Although the original model, in which the scalar field is minimally coupled to gravity, is now disfavored by current observational constraints, some variants of natural inflation, including the generalized and multi-field versions, were proposed and discussed in Refs. [14,29–32], and references therein. The inflationary predictions in those extended models can be modified and, in general, be consistent with observations.

Adopting the original natural inflation potential without any modification – e.g., $V(\phi) = \Lambda^4[1 + \cos(\phi/f)]$, we investigate natural inflation for the cosmological models with the derivative self-interaction of the inflaton field and inflaton's kinetic coupling to gravity via the Einstein tensor. The cosmological model of our interest was proposed in Ref. [33] (see Refs. [34,35] for its applications) as a subclass of *G*-inflation framework [36], which is based on the Horndeski (equivalently, generalized Galileon) theory [37,38], *i.e.*, the most general scalar-tensor theory with second-order field equations avoiding the Ostrogradski instability [39], see Ref. [40] for a review. A unique feature of considering inflaton's derivative self-interaction and its kinetic coupling with gravity is that the gravitationally enhanced friction mechanism works for steep potentials [41–46]. Thus, it motivates us to investigate whether it is possible to reconcile the predictions of natural inflation with the CMB observations in the setting of inflaton's derivative self-interaction and its kinetic coupling with gravity scenario.

After inflation, it is usually assumed that the inflaton coherently oscillates at the minimum of its potential, decaying and transferring its energy to a relativistic plasma of the standard model particles [47–49]. This post-inflationary process that populates our universe with ordinary matter is known as *reheating*, see Ref. [50] for a review. Because there are no direct cosmological observations are traceable

from reheating, the physics of reheating is highly uncertain and unconstrained. Thus, this post-inflationary era depends heavily on models of inflation. It was pointed out in the literature that consideration of reheating may provide additional constraints to inflationary perdictions [51–55]. In this work, for our model, we follow the approaches proposed in Refs. [29,51–58] to perform the analyses on the reheating parameters, including the equation of state, the duration, and the temperature of reheating. Then, using the link between these parameters of reheating and the observable quantities of inflation, we provide constraints on the inflationary predictions of natural inflation in light of current observational data [10,11,28].

This paper is organized as follows. We start Sect. 2 by setting up our model with the derivative self-interaction of the scalar field and the kinetic coupling between the scalar field and gravity, which belongs to the subclass of Horndeski's theory of gravity. Then, in the same section, we derive the background equations of motion, as well as the observable quantities; including power spectra of tensor and scalar modes, $\mathcal{P}_S$ and $\mathcal{P}_T$, respectively, their spectral tilts n_S and n_T, and the tensor-to-scalar ratio r in the slow-roll scenario of inflation. Based on our analytic results obtained in Sect. 2, we place the observational constraints on n_S and r predictions of natural inflation in Sect. 3 and show that the natural inflation model is now consistent with the latest observational data, mainly due to the suppressed tensor-to-scalar ratio. In Sect. 4, we impose the effects of reheating to the predictions of natural inflation. The results of the section implies that the reheating parameters, the equation of state ω_{re} and the temperature T_{re} at the end of reheating, significantly affect the duration of inflation N_k hence the n_S and r. We conclude our work and provide some implications of our findings in Sect. 5.

2 Background and perturbation dynamics

The action for the cosmological model that we investigate in this work is give as [33–35]

$$S = \int d^4x \sqrt{-g} \left[\frac{M_p^2}{2} R - \frac{1}{2} \left(g^{\mu\nu} - \frac{\alpha}{M^3} g^{\mu\nu} \partial_\rho \partial^\rho \phi \right. \right.$$
$$\left. \left. + \frac{\beta}{M^2} G^{\mu\nu} \right) \partial_\mu \phi \partial_\nu \phi - V(\phi) \right], \tag{1}$$

where $M_p = 2.44 \times 10^{18}$ GeV is the reduced Planck mass and $V(\phi)$ is the inflaton potential, and M is the mass scale making α and β dimensionless constants. In the limit $(\alpha, \beta) \to 0$, the Einstein gravity with a minimal coupling to the scalar field is recovered. Thus, the case with $(\alpha, \beta) \neq 0$ reflects the deviation from the general relativity. While Refs. [33–35]

discuss the scalar field dependent coupling function $\xi(\phi)$ for the α-term in Eq. (1), we consider such the coupling to be a constant; namely, $\xi(\phi) = 1$, in the present study for simplicity.

Varying the action with respect to metric $g_{\mu\nu}$ and ϕ, one obtains the Einstein and field equations

$$G_{\mu\nu} = \frac{1}{M_p^2} T_{\mu\nu}, \tag{2}$$

$$\partial_\mu \partial^\mu \phi - V_{,\phi} + \frac{\alpha}{M^3} \left(\partial_\mu \partial_\nu \phi \partial^\mu \partial^\nu \phi - \partial_\mu \partial^\mu \phi \partial_\nu \partial^\nu \phi \right.$$
$$\left. + R_{\mu\nu} \partial^\mu \partial^\nu \phi \right) + \frac{\beta}{M^2} G_{\mu\nu} \partial^\mu \partial^\nu \phi = 0, \tag{3}$$

respectively, where the $G_{\mu\nu} = R_{\mu\nu} - g_{\mu\nu} R/2$ is the Einstein tensor,

$$T_{\mu\nu} = \partial_\mu \phi \partial_\nu \phi - \frac{1}{2} g_{\mu\nu} \left(\partial_\alpha \phi \partial^\alpha \phi + 2V \right)$$
$$+ \frac{\alpha}{M^3} \left[(\partial_\alpha \phi \partial^\alpha \phi)_{(\mu} \partial_{\nu)} \phi - \Box \phi \partial_\mu \partial_\nu \phi \right.$$
$$\left. - \frac{1}{2} g_{\mu\nu} (\partial_\alpha \phi \partial^\alpha \phi)_\beta \partial^\beta \phi \right]$$
$$+ \frac{\beta}{M^2} \left[-\frac{1}{2} \partial_\mu \phi \partial_\nu \phi R + 2 \partial_\alpha \phi \partial_{(\mu} \phi R^\alpha{}_{\nu)} \right.$$
$$+ \partial^\alpha \phi \partial^\beta \phi R_{\mu\alpha\nu\beta} + \partial_\mu \partial^\alpha \phi \partial_\nu \partial_\alpha \phi - \partial_\mu \partial_\nu \phi \Box \phi$$
$$- \frac{1}{2} G_{\mu\nu} \partial_\alpha \phi \partial^\alpha \phi + \frac{1}{2} g_{\mu\nu} \left((\Box \phi)^2 \right.$$
$$\left. \left. - \partial^\alpha \partial^\beta \phi \partial_\alpha \partial_\beta \phi - 2 \partial_\alpha \phi \partial_\beta \phi R^{\alpha\beta} \right) \right], \tag{4}$$

is the energy momentum tensor, $\Box \phi \equiv \partial_\mu \partial^\mu \phi$, and $V_{,\phi} \equiv dV(\phi)/d\phi$. In a spatially flat Friedman-Robertson-Walker universe with metric

$$ds^2 = -dt^2 + a(t)^2 \delta_{ij} dx^i dx^j, \tag{5}$$

where $a(t)$ is a scale factor, the background and field equations are obtained as

$$3M_p^2 H^2 = \frac{1}{2} \dot{\phi}^2 + V(\phi) + \frac{3\alpha}{M^3} H \dot{\phi}^3 - \frac{9\beta}{2M^2} \dot{\phi}^2 H^2, \tag{6}$$

$$M_p^2 \left(2\dot{H} + 3H^2 \right) = -\frac{1}{2} \dot{\phi}^2 + V + \frac{\alpha}{M^3} \dot{\phi}^2 \ddot{\phi}$$
$$- \frac{\beta}{2M^2} \dot{\phi}^2 \left(2\dot{H} + 3H^2 + 4H \frac{\ddot{\phi}}{\dot{\phi}} \right), \tag{7}$$

$$\ddot{\phi} + 3H\dot{\phi} + V_{,\phi} + \frac{3\alpha}{M^3} \dot{\phi}^2 \left(\dot{H} + 3H^2 + 2H \frac{\ddot{\phi}}{\dot{\phi}} \right)$$
$$- \frac{3\beta}{M^2} H\dot{\phi} \left(2\dot{H} + 3H^2 + H \frac{\ddot{\phi}}{\dot{\phi}} \right) = 0, \tag{8}$$

where the overdot denotes the derivative with respect to time t. To investigate the slow-roll inflation, we take so called the slow-roll conditions that read $V(\phi) \gg \dot{\phi}^2$ and $\ddot{\phi} \ll 3H\dot{\phi}$

into account and introduce the following slow-roll parameters

$$\epsilon_1 \equiv -\frac{\dot{H}}{H^2}, \quad \epsilon_2 \equiv -\frac{\ddot{\phi}}{H\dot{\phi}}, \quad \epsilon_3 \equiv \frac{\dot{\phi}^2}{2M_p^2 H^2}, \tag{9}$$

which assumed to be small, $\epsilon_i \ll 1$ where $i = 1, 2, 3$, during inflation. Equation (8) can, therefore, be rewritten in terms of these parameters as

$$3H\dot{\phi} \left[1 - \frac{1}{3} \epsilon_2 + \frac{3\alpha}{M^3} H\dot{\phi} \left(1 - \frac{\epsilon_1}{3} - \frac{2\epsilon_2}{3} \right) \right.$$
$$\left. - \frac{3\beta}{M^2} H^2 \left(1 - \frac{2\epsilon_1}{3} - \frac{\epsilon_2}{3} \right) \right] = -V_{,\phi}. \tag{10}$$

Thus, under the slow-roll conditions, Eqs. (6) and (8) can be approximated as

$$3M_p^2 H^2 \simeq V, \quad 3H\dot{\phi} (1 + \mathcal{A}) \simeq -V_{,\phi}, \tag{11}$$

where

$$\mathcal{A} = \frac{3\alpha}{M^3} H\dot{\phi} - \frac{3\beta}{M^2} H^2. \tag{12}$$

In Eq. (11), $(1 + \mathcal{A})$ should be positive not to violate the null energy condition. As one can see from Eq. (12) that the function $\mathcal{A}$ encodes the information about the additional interactions; the derivative self-interaction of the scalar field (the first term) and the kinetic coupling between the scalar field and gravity (the second term) that we introduced in Eq. (1), and it becomes zero if both terms cancel each other, which indicates the complete absence of these additional interactions in our model. To weigh the contributions of each term in Eq (12) during inflation, we introduce a parameter defined by

$$\gamma \equiv \frac{\alpha}{\beta M} \frac{\dot{\phi}}{H}. \tag{13}$$

If the kinetic coupling between the scalar field and gravity is much stronger (or weaker) than the derivative self-interaction of the scalar field during inflation, $|\gamma| \ll 1$ (or $|\gamma| \gg 1$). Thus, the equally important contributions from both interactions indicate $|\gamma| \sim \mathcal{O}(1)$. Equation (12) can be rewritten in terms of γ as

$$\mathcal{A} = 3\beta(\gamma - 1) \frac{H^2}{M^2}. \tag{14}$$

Here, if the γ equals unity, the $\mathcal{A}$ becomes zero, which, as discussed, indicates the absence of the additional interactions. The resulting spectrum for the CMB mode would be the same as that in slow-roll inflation in GR. If the $\mathcal{A}$ is non-zero, one can consider two different limiting cases; $|\mathcal{A}| \ll 1$ and $\mathcal{A} \gtrsim 1$, respectively, during inflation. When

$|\mathcal{A}| \ll 1$, Eq. (11) leads to the slow-roll approximated equations for standard single-field inflation in the Einstein gravity. Although the $|\mathcal{A}| \ll 1$ case could be interesting to investigate as it can be treated perturbatively in the slow-roll parameters, its effect deviating from standard slow-roll inflation in general relativity (GR) would be small, if not negligible. It is, therefore, worth investigating the second case where $\mathcal{A} \gtrsim 1$ to account for the effects of additional interactions encoded in the $\mathcal{A}$. Thus, our interest in this work is to consider the case where $\mathcal{A} \gtrsim 1$, while $|\gamma| \sim \mathcal{O}(1)$. From Eq. (14), condition $\mathcal{A} \gtrsim 1$ implies that

$$\frac{H^2}{M_p^2} \gtrsim \frac{1}{3\beta(\gamma - 1)} \frac{M^2}{M_p^2}, \tag{15}$$

where $\beta(\gamma - 1) > 0$ with $|\gamma| \sim \mathcal{O}(1)$ is assumed. To satisfy the sufficient condition to avoid from quantum gravity that reads $H^2/M_p^2 \ll 1$, the condition $M^2/M_p^2 \ll 3\beta(\gamma - 1)$ should also hold for our model, and we will examine the parameter space that satisfies this condition in the next section.

The amount of inflation is quantified by the number N_k of e-folds, which reads

$$N_k = \int_\phi^{\phi_e} \frac{H}{\dot{\tilde{\phi}}} d\tilde{\phi} \simeq \frac{1}{M_p^2} \int_{\phi_e}^\phi \frac{V}{V_{,\tilde{\phi}}} (1 + \mathcal{A}) \, d\tilde{\phi}, \tag{16}$$

where ϕ_e is the scalar-field value at the end of inflation and is to be estimated by solving $\epsilon_1(\phi_e) \equiv 1$.

The linear perturbation analysis for our model Eq. (1) is carried out in Refs. [33,35], see Ref. [36] for more general cases, and the observable quantities, including power spectra of the scalar ($\mathcal{P}_S$) and tensor ($\mathcal{P}_T$) modes, their spectral tilts (n_S and n_T, respectively), and the tensor-to-scalar ratio r, are computed on the large scale $c_S k|\tau| \ll 1$ as

$$\mathcal{P}_S = \frac{k^3}{2\pi^2} \left| \frac{v_k}{z_S} \right|^2 \simeq \frac{H^2}{8\pi^2 M_p^2 c_S^3 \epsilon_V} (1 + \mathcal{A}), \tag{17}$$

$$\mathcal{P}_T = \frac{k^3}{\pi^2} \sum_{\lambda = x,+} \left| \frac{\mu_{\lambda,k}}{z_T} \right|^2 \simeq \frac{H^2}{2\pi^2 M_p^2 c_T^3}, \tag{18}$$

$$n_S - 1 = \frac{d \ln \mathcal{P}_S}{d \ln k} = 3 - 2\mu_S$$
$$\simeq \frac{1}{1 + \mathcal{A}} \left[2\eta_V - 2\epsilon_V \left(4 - \frac{1}{1 + \mathcal{A}} \right) \right], \tag{19}$$

$$n_T = \frac{d \ln \mathcal{P}_T}{d \ln k} = 3 - 2\mu_T \simeq -\frac{2\epsilon_V}{1 + \mathcal{A}}, \tag{20}$$

$$r = \frac{\mathcal{P}_T}{\mathcal{P}_S} \simeq \frac{16\epsilon_V}{1 + \mathcal{A}}, \tag{21}$$

where $\epsilon_V \equiv M_p^2 \left(V_{,\phi}/V \right)^2 / 2$ and $\eta_V \equiv M_p (V_{,\phi\phi}/V)$, and $c_{S,T}^2 \sim 1 + \mathcal{O}(\epsilon_1) \simeq 1$, see Refs. [33,35] for further details.

Based on these findings, we place observational constraints on the natural inflation model in the following sections. In the standard single field inflation scenario in the general relativity, which is $\mathcal{A} \ll 1$ limit of our model, the theoretical predictions of natural inflation on n_S and r has been disfavored by observational data [10,11,28]. Thus, in the following section, we place observational constraints on natural inflation in the $\mathcal{A} \gg 1$ limit and show that the model is now consistent with the current observations even at 1σ (68% confidence) level.

3 Observational constraints

In the presence of the derivative self-interaction of the scalar field and its kinetic coupling with the Einstein tensor, we place observational constraints on natural inflation. Since natural inflation in the GR limit, where $\mathcal{A} = 0$ (equivalently, $\gamma = 1$), is well discussed in Refs. [10,11,26,27] and references therein, we investigate the $\mathcal{A} \gg 1$ case, from now on, to account for the significant deviation from the standard slow-roll inflation scenario in GR. In this and next section, we consider the $\mathcal{A} \gg 1$ limit of our analytic results of the previous section. Thus, it is worth emphasizing that results in this and the following sections correspond only to the $\gamma \neq 1$ case.[1] The potential for natural inflation reads

$$V(\phi) = \Lambda^4 \left[1 + \cos \left(\frac{\phi}{f} \right) \right], \tag{22}$$

where the energy density Λ^4 and the decay constant f are the parameters of the model with dimensions of mass. In the limit $f \to \infty$, the potential behaves like pure power laws, e.g., $V(\phi) \sim m^2 \phi^2$ where m is an energy scale that plays the role of Λ [29]. For natural inflation, the number N_k of e-fold is obtained from Eq. (16) as

$$N_k = \Delta \left[\mathcal{F}(\phi_e) - \mathcal{F}(\phi) \right], \tag{23}$$

where

$$\Delta = \beta(\gamma - 1) \frac{f^2 \Lambda^4}{M^2 M_p^4}, \tag{24}$$

and

$$\mathcal{F}(\phi) = \cos \left(\frac{\phi}{f} \right) + 4 \ln \sqrt{\pm \frac{1}{2} \left[1 - \cos \left(\frac{\phi}{f} \right) \right]}. \tag{25}$$

---

[1] Taking the $\gamma \to 1$ limit for our results in this and next sections does not reproduce the standard results. In other words, the $\gamma = 1$ (or $\mathcal{A} = 0$) case should be treated separately.

Here, we choose "+" sign in Eq. (25) since the quantity under the square root should be positive. To obtain Eq. (23), we assumed $\mathcal{A} \gg 1$ in Eq. (16). By using the condition that $\epsilon_1(\phi_e) = 1$, we obtain the scalar-field value ϕ_e at the end of inflation as

$$\cos\left(\frac{\phi_e}{f}\right) = \frac{4}{1 \pm \sqrt{16\Delta + 1}} - 1, \tag{26}$$

where we choose "+" sign for reason that $|\cos(\phi_e/f)| \leq 1$. Substituting Eq. (26) into Eq. (25), we obtain

$$\mathcal{F}(\phi_e) = 2\ln\left[\frac{1 + 8\Delta - \sqrt{16\Delta + 1}}{8\Delta}\right] - \frac{1 + 4\Delta - \sqrt{16\Delta + 1}}{4\Delta}. \tag{27}$$

Consequently, the potential value at the end of inflation gets

$$V(\phi_e) = \left(\frac{\sqrt{16\Delta + 1} - 1}{4\Delta}\right) \Lambda^4. \tag{28}$$

For the potential in Eq. (22), the spectral index for scalar modes and the tensor-to-scalar ratio are obtained from Eqs. (19) and (21) as

$$n_S = 1 - \frac{2\left[2 - \cos\left(\frac{\phi}{f}\right)\right]}{\Delta\left[1 + \cos\left(\frac{\phi}{f}\right)\right]^2}, \tag{29}$$

$$r = \frac{8\left[1 - \cos\left(\frac{\phi}{f}\right)\right]}{\Delta\left[1 + \cos\left(\frac{\phi}{f}\right)\right]^2}. \tag{30}$$

Using Eq. (23), we obtain

$$\cos\left(\frac{\phi}{f}\right) = 1 + 2\mathcal{W}\left(\pm e^{\frac{1}{2}\left(\mathcal{F}(\phi_e) - \frac{N_k + \Delta}{\Delta}\right)}\right), \tag{31}$$

where $\mathcal{W}(x)$ is the product logarithm function, also known as the Lambert $\mathcal{W}$ function, and both Δ and N_k are positive constants. Let us first consider the positive sign for the argument of $\mathcal{W}$-function in Eq. (31). As the Δ increases from 0 to ∞, while the number of e-folds of inflation is fixed to be $N_k \sim 60$, the exponent increases from $-\infty$ to -1, see the left panel of Fig. 1. Thus, the argument of $\mathcal{W}(x)$ takes a value in a range $0 \leq x \leq 1/e$ and, consequently, the $\mathcal{W}(x)$ takes a value between zero and $\mathcal{W}(1/e) \simeq 0.2784$. As a result from Eq. (31), we obtain $\cos(\phi/f) \geq 1$, and the scalar field becomes complex-valued, which we are not interested in in this work. Let us now consider the negative sign in Eq. (31). Again, as the Δ increases from 0 to ∞ for a fixed N_k, the argument of $\mathcal{W}(x)$ decreases in a range $0 \geq x \geq -1/e$. In that case, there are two branches of real values of $\mathcal{W}(x)$. Following Ref. [59], we denote the branch satisfying $\mathcal{W}(x) \leq -1$ by $\mathcal{W}_{-1}(x)$ and the branch satisfying $-1 \leq \mathcal{W}(x) \leq 0$ by $\mathcal{W}_0(x)$. For the $\mathcal{W}_{-1}(x)$ branch, we obtain $\cos(\phi/f) \leq -1$ from Eq. (31), in which the scalar field is also complex-valued. Lastly, we obtain $|\cos(\phi/f)| \leq 1$ for the $\mathcal{W}_0(x)$ branch. Thus, for our further study, we choose the negative sign in Eq. (31) and the $\mathcal{W}_0(x)$ branch where $-1 \leq \mathcal{W}(x) \leq 0$, and then $|\cos(\phi/f)| \leq 1$, see the right panel of Fig. 1.

Although we have several free parameters; including α, β, and M, coming from our model, and Λ and f, from the choice of inflaton potential, our result shows that the theoretical predictions of n_S and r depend only on a single parameter Δ, which is given in Eq. (24). Thus, it is effectively one parameter model, and we plot in the left panel of Fig. 2 the theoretical predictions of our model based on Eqs. (29) and (30) for natural inflation.

The shaded dark- and light-blue regions represent the 1σ and 2σ confidence contours of the Planck+BICEP/Keck 2018 data [28], respectively. The diagonal gray lines indicate the different values of Δ; for example, $\Delta = 20$ for the orange line. The purple lines represent the number N_k of e-
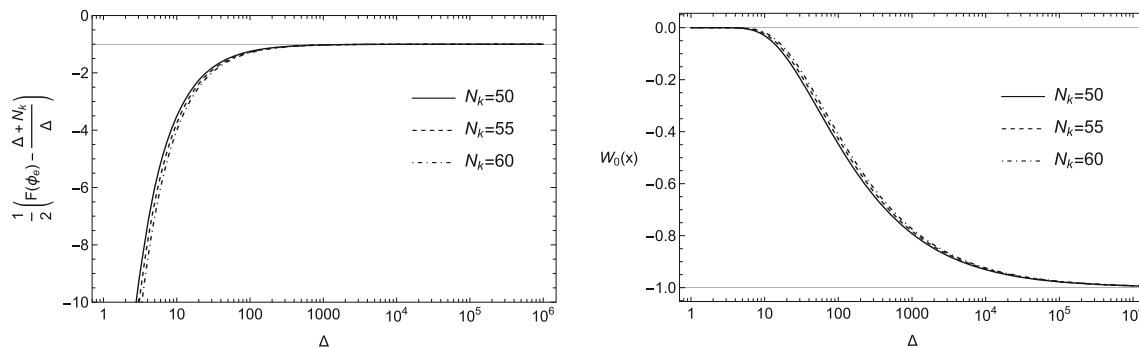

Fig. 1 Left: the exponent of an argument of $\mathcal{W}$-function in Eq. (31) as a function of Δ and N_k. The solid, dashed, and dot-dashed lines correspond to $N_k = 50$, 55, and 60, respectively. The the exponent grows from $-\infty$ to -1, the horizontal black solid line, as the Δ increases from 0 to ∞. Right: the $\mathcal{W}_0(x)$ branch as a function of Δ and N_k, which gives $|\cos(\phi/f)| \leq 1$ in Eq. (31)

folds during inflation; $N_k = 50$ (dotted), 60 (dashed), and 70 (solid). The values of r and n_S decrease/increase along the purple lines as the Δ value decreases/increases. The figure shows that natural inflation is now compatible with the observational data if the kinetic coupling between gravity and the scalar field and the derivative self-interaction of the scalar field are taken into account during inflation. For our model to be consistent with the observational data at $1\sigma/2\sigma$ level, the duration of inflation is preferred to be $N_k \gtrsim 60/N_k \gtrsim 50$. The ranges of Δ compatible with the data are $18 \lesssim \Delta \lesssim 25$ (1σ confidence) and $25 \lesssim \Delta \lesssim 45$ (2σ confidence) for $N_k = 60$(dashed line), the most conservative value for duration of inflation. Having obtained the range of Δ values in agreement with the observational data, we can search for the parameter space of other parameters using Eq. (24).

The amplitude of the scalar power spectrum is well determined to be $\mathcal{P}_S(k_*) = 2.0989 \times 10^{-9}$ (TT, TE, EE + lowE + lensing) at the pivot scale $k_* = 0.05\,\text{Mpc}^{-1}$ [10,11]. Thus, we can use Eq. (17) to obtain the Λ parameter. First, we write Eq. (17) in the following form

$$\mathcal{P}_S(k_*) = \frac{\Delta}{12\pi^2}\frac{\Lambda^4}{M_p^4}\left[1 + \cos\left(\frac{\phi}{f}\right)\right]^3\left[1 - \cos\left(\frac{\phi}{f}\right)\right]^{-1}$$
$$= 2.0989 \times 10^{-9}, \tag{32}$$

where $\cos(\phi/f)$ is given in Eq. (31) in terms of N_k and Δ. The N_k can be expressed in terms of n_S and Δ after substituting Eq. (31) into Eq. (29), which then reads

$$N_k = \Delta\left\{\mathcal{F}(\phi_e) - \ln\left[\exp\left(\frac{1 - (n_S - 1)\Delta + \sqrt{1 - 6(n_S - 1)\Delta}}{(n_S - 1)\Delta}\right)\right.\right.$$
$$\left.\left.\times \left(\frac{1 - 2(n_S - 1)\Delta + \sqrt{1 - 6(n_S - 1)\Delta}}{2(n_S - 1)\Delta}\right)^2\right]\right\}. \tag{33}$$

Thus, we obtain $\Lambda(n_S, \Delta)$ from Eq. (32) as

$$\frac{\Lambda^4}{M_p^4} = -\frac{3\pi^2}{\Delta}\mathcal{P}_S(k_*)\left(1 + \mathcal{W}\left[-\sqrt{\exp\left(\mathcal{F}(\phi_e) - \frac{N_k + \Delta}{\Delta}\right)}\right]\right)^{-3}$$
$$\times \mathcal{W}\left[-\sqrt{\exp\left(\mathcal{F}(\phi_e) - \frac{N_k + \Delta}{\Delta}\right)}\right]. \tag{34}$$

For the central $n_S = 0.9649$ value from the Planck TT, TE, EE + lowE + lensing data [10,11], Eq. (34) gives $2.7331 \times 10^{-3} \leq \Lambda/M_p \leq 5.1006 \times 10^{-3}$ for the $15 \leq \Delta \leq 28$ range. The corresponding range of tensor-to-scalar ratio is $0.0035 \leq r \leq 0.036$, which is compatible with the latest constraint on $r_{0.05} < 0.036$ at 95% confidence [28].

Substituting Eq. (34) into Eq. (24), we plot the parameter space of $\beta(\gamma - 1)$ vs. M^2/M_p^2 in the right panel of Fig. 2. The black solid line indicates cutoff scale $M^2/M_p^2 = 3\beta(\gamma - 1)$. The gray shaded region presents the allowed parameter space from Eq. (15) satisfying the sufficient condition $M^2/M_p^2 \ll 3\beta(\gamma - 1)$ to avoid the quantum gravity. For plotting the blue- and red-shaded regions, we adopt the $n_S = 0.9649$ and $0.3 \leq \log_{10}(f/M_p) \leq 2.5$ from the Planck paper [10,11]. The value of f/M_p increases from solid to dashed boundaries, while we set $\Delta = 15$ and $\Delta = 28$ for the blue and red regions, respectively. Since we consider $\gamma \neq 1$ case; hence $\beta \neq 0$, in this study, the divergence occurring at $\beta(\gamma - 1) = 0$
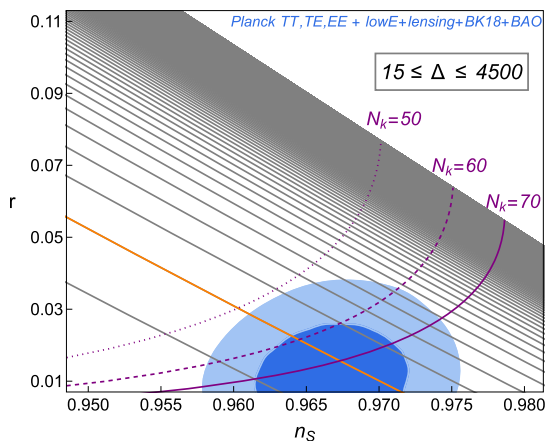

Fig. 2 Left: the $n_S - r$ plot for natural inflation with potential given in Eq. (22). The shaded regions present the 1σ (dark blue) and 2σ (light blue) contours of the latest Planck+BICEP/Keck 2018 data [28]. The diagonal gray lines indicate the different values of Δ within the interval $15 \leq \Delta \leq 4500$, increasing from bottom left to top right with a step of 10. For the orange line, $\Delta = 20$. The purple lines represent the number N_k of e-folds during inflation; $N_k = 50$ (dotted), 60 (dashed), and 70 (solid). Right: the parameter space of $\beta(\gamma - 1)$ vs.
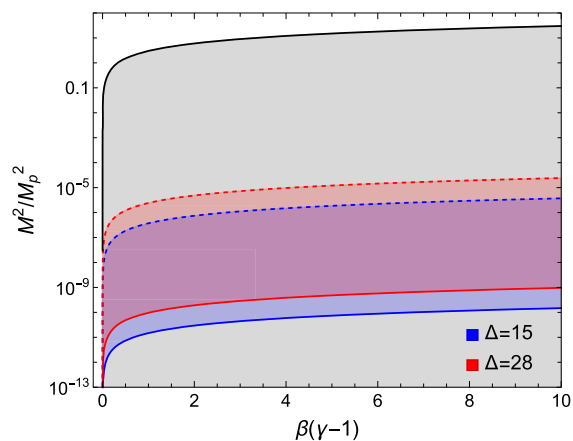
M^2/M_p^2 from Eq. (24), where the black line corresponds to the cutoff scale $M^2/M_p^2 = 3\beta(\gamma - 1)$. The gray shaded region is the allowed parameter space satisfying $M^2/M_p^2 \lesssim 3\beta(\gamma - 1)$. For the blue- and red-shaded regions, we set $\Delta = 15$ and $\Delta = 28$, respectively, and vary the f/M_p value within the range of $0.3 \leq \log_{10}(f/M_p) \leq 2.5$ adopted from Planck paper [10,11], the value increases from solid to dashed boundaries

is not physical. In other words, the $\gamma = 1$ case should be treated separately. The left panel of Fig. 2 shows that the CMB data prefer the positive values of Δ, which indicates the $\beta(\gamma - 1)$ in Eq. (24) must also be positive. Therefore, $\beta > 0$ for $\gamma > 1$ and $\beta < 0$ for $\gamma < 1$ in the right panel of Fig. 2, respectively. Thus, we conclude from Fig. 2 that the natural inflation model is now consistent with the latest observational data for a broad range of model parameters. In the following section, to put further constraints to the inflationary predictions for natural inflation, we impose reheating considerations after inflation.

4 Reheating constraints

Inflation ends when equation-of-state parameter becomes $\omega_{\text{inf}} = -1/3$. The standard inflationary cosmology then assumes that, after inflation, the universe undergoes a phase of reheating, during which the inflaton field coherently oscillates at the minimum of its potential, decaying and transferring its energy to a relativistic plasma, and populates the universe with ordinary matter. As for the reheating phase, we follow the approaches proposed in Refs. [29,51–58], especially [29,56], in which the present day observations are related to the evolution of the inflaton field during inflation. The key is the relation between the comoving scale k today and that during inflation. In other words, the comoving Hubble radius, $a_k H_k = k$, exiting the horizon is associated with that of present time by

$$\ln \frac{k}{a_0 H_0} = \ln \frac{(aH)_k}{(aH)_e} + \ln \frac{(aH)_e}{(aH)_{re}} + \ln \frac{(aH)_{re}}{(aH)_{eq}} + \ln \frac{(aH)_{eq}}{a_0 H_0}.$$
(35)

The number of e-folds during each inflation, reheating, and radiation dominated epoch; $N_k = \ln(a_e/a_k)$, $N_{re} = \ln(a_{re}/a_e)$, and $N_{RD} = \ln(a_{eq}/a_{re})$, respectively, can be used to simplify Eq. (35) as

$$\ln \frac{k}{a_0 H_0} = -N_k - N_{re} - N_{RD} + \ln \frac{a_{eq}}{a_0} + \ln \frac{H_k}{H_0},$$
(36)

where "a_{eq}" is the scale factor at the matter and radiation equality, and the subscript "0" denotes the present day value of each quantity. The Hubble parameter during inflation is obtained from Eq. (18) with an assumption $\mathcal{P}_T(k_*) = r\mathcal{P}_S(k_*)$ to be $H_k = \sqrt{2}\pi M_p (r\mathcal{P}_S)^{1/2} c_T^{3/2}$, where $c_T \simeq 1$ for our case. The ratio between the energy density ρ_e at the end of the inflation and the energy density ρ_{re} at the end of the reheating depends on the equation-of-state parameter and the duration of reheating and is

$$\frac{\rho_{re}}{\rho_e} = e^{-3(1+\omega_{re})N_{re}}.$$
(37)

The energy density ρ_e at the end of inflation is then computed from the modified Friedmann equations Eq. (11) to be $\rho_e \simeq V(\phi_e)$. Assuming the conservation of entropy and the current neutrino temperature, $T_{\nu,0} = (4/11)^{1/3} T_0$, the energy density at reheating is

$$\rho_{re} = \frac{\pi^2 g_{re}}{30} T_{re}^4,$$
(38)

where

$$T_{re} = \left(\frac{43}{11 g_{s,re}}\right)^{\frac{1}{3}} \frac{a_0}{a_{re}} T_0.$$
(39)

The number of e-folds during reheating can be obtained from Eq. (37) with Eqs. (38) and (36) as

$$N_{re} = \frac{4}{1-3\omega_{re}} \left[-N_k - \ln \frac{k}{a_0 T_0} - \frac{1}{4} \ln \frac{30}{\pi^2 g_{re}} - \frac{1}{3} \ln \frac{11 g_{s,re}}{43} \right.$$
$$\left. - \frac{1}{4} \ln V(\phi_e) + \frac{1}{2} \ln \left(2\pi^2 M_p^2 r \mathcal{P}_S\right) \right].$$
(40)

The corresponding reheating temperature, T_{re}, is

$$T_{re}^4 = \left(\frac{30}{\pi^2 g_{re}}\right) V(\phi_e) e^{-3(1+\omega_{re})N_{re}}.$$
(41)

Assuming the effective equation-of-state parameter ω_{re} is functionally constant, we plot the temperature T_{re} and the duration of reheating as functions of the spectral index n_S in Fig. 3. The left and right panels correspond to two different values of Δ. In each figure, we choose four different values of ω_{re}; namely, $\omega_{re} = -1/3$ (red), $\omega_{re} = 0$ (blue), $\omega_{re} = 0.25$ (black), and $\omega_{re} = 1$ (green). The smallest $\omega_{re} = -1/3$ value is required for inflation end, while the largest $\omega_{re} = 1$ one, the most conservative upper limit, comes from the causality. Thus, the ω_{re} value varies within the interval of $-1/3 \leq \omega_{re} \leq 1$. The background yellow shaded region presents the current 1σ range of $n_S = 0.9649 \pm 0.0042$ (68%, $TT, TE, EE + lowE + lensing$) from Planck data [10,11]. The pink and brown shaded regions with $T_{re} \leq 100$GeV and $T_{re} \leq 10$ MeV indicate the constraints on energy scales the electroweak and the big-bang nucleosynthesis, respectively. The ω_{re} values residing inside the shaded regions are favored. The curves of all ω_{re} intersect at $(n_S, T_{re}^{max}) = (0.9634, 3.04 \times 10^{15}\text{GeV})$ for $\Delta = 20$ and $(n_S, T_{re}^{max}) = (0.9698, 3.26 \times 10^{15}\text{GeV})$ for $\Delta = 40$ and indicate the instantaneous reheating ($N_{re} = 0$) for our model. The instantaneous reheating temperature T_{re}^{max} and corresponding spectral index n_S values slightly increase as the Δ value increases, which is due to the potential energy value at the end of inflation depends on the value of Δ, see Eqs. (28) and (41). By matching the lines of the same colors
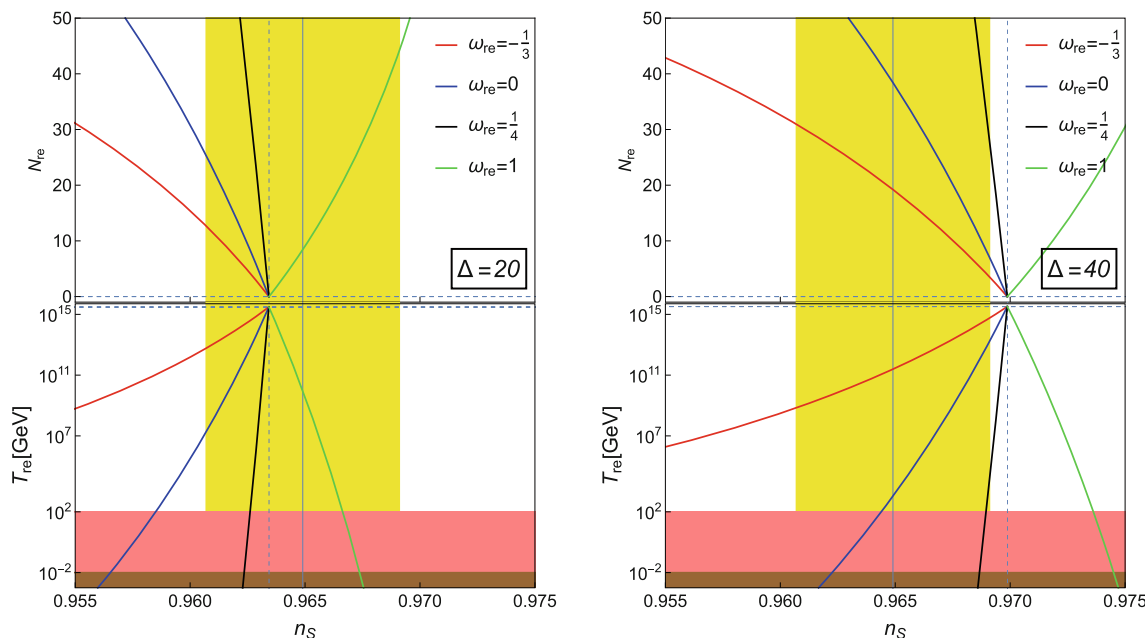
Fig. 3 The $n_S - T_{re}$ (bottom) and $n_S - N_{re}$ (top) plots for natural inflation with potential given in Eq. (22). The yellow shaded region indicates the current 1σ range of $n_S = 0.9649 \pm 0.0042$ ($68\%, TT, TE, EE + lowE + lensing$) from Planck data [10,11]. The pink and brown shaded regions indicate the $T_{re} \leq 100 \text{GeV}$ and $T_{re} \leq 10 \text{MeV}$ energy scales, respectively. The ω_{re} values residing inside the shaded regions are favored

in both upper and lower panels, one can estimate the duration and corresponding temperature of reheating. Thus, for given ω_{re}, the figure shows that the longer the reheating lasts, the lower the temperature gets at the end of reheating. For the increasing direction of n_S, the T_{re} increases, while the N_{re} decreases, toward the intersecting point for $\omega_{re} < 1/3$. As for the case of $\omega_{re} > 1/3$, the T_{re} decreases, while N_{re} increases, away from the intersecting point of all lines.

In Eq. (33), the duration N_k of inflation is expressed in terms of n_S and Δ. Also, the n_S can be expressed in terms of reheating parameters, including ω_{re}, N_{re}, and T_{re}. Thus, by taking the reheating considerations into account, we plot $n_S - r$ predictions once again in Fig. 4 for the same values of ω_{re} as Fig. 3. Since N_{re} and T_{re} are related to each other, we choose T_{re} as another reheating parameter in Fig. 3. As it is in Fig. 2, the underlying diagonal gray lines correspond to the different values of Δ, and it increases from bottom left to top right within the interval of $20 \leq \Delta \leq 40$. The purple lines are some reference values of N_k. As the labels indicate in each panel, the different colors on the diagonal lines correspond to the different values of T_{re}. The main implication of this figure is that both the ω_{re} and the T_{re} at the end of reheating provide us with information about how long inflation had to be lasted to be compatible with the CMB observations. For example, if $\omega_{re} < 1/3$, inflation cannot last longer than $N_k \simeq 57$ e-folds due to our reheating considerations. Thus, the prediction of n_S and r is only 2σ

consistent with the observations. Conversely, the duration of inflation must be longer than $N_k \gtrsim 57$ for $\omega_{re} > 1/3$. As a result, the theoretical prediction of our model is still consistent with the CMB data, the n_S and r values residing inside 1σ contour. The turning point is the instantaneous reheating with $N_{re} = 0$, which also indicates $\omega_{re} = 1/3$. Since reheating must have occurred instantaneously after inflation, the estimated duration of inflation is $N_k \simeq 57$ e-folds, the exact value is slightly different for different Δ values as the figure shows. Figure 4 also shows that the CMB data prefer different ranges of reheating temperature depending on the values of ω_{re}. For equation of state approaching $\omega_{re} \simeq 1/3$, the reheating temperature from as low as a few MeV to as large as 10^{15}GeV can be achieved.

5 Conclusions

For a cosmological model described by Eq. (1), where the derivative self-interaction of a scalar field and its kinetic coupling with gravity is presented, we placed observational constraints on the natural inflation model. Then, we investigated the effects of reheating on the inflationary predictions. The interactions we introduced in this work are assumed to give equally important contributions during inflation such that $|\gamma| \sim \mathcal{O}(1)$ in Eq. (13). The main analytic results of inflationary predictions for our model are obtained in Eqs. (17)–(21),
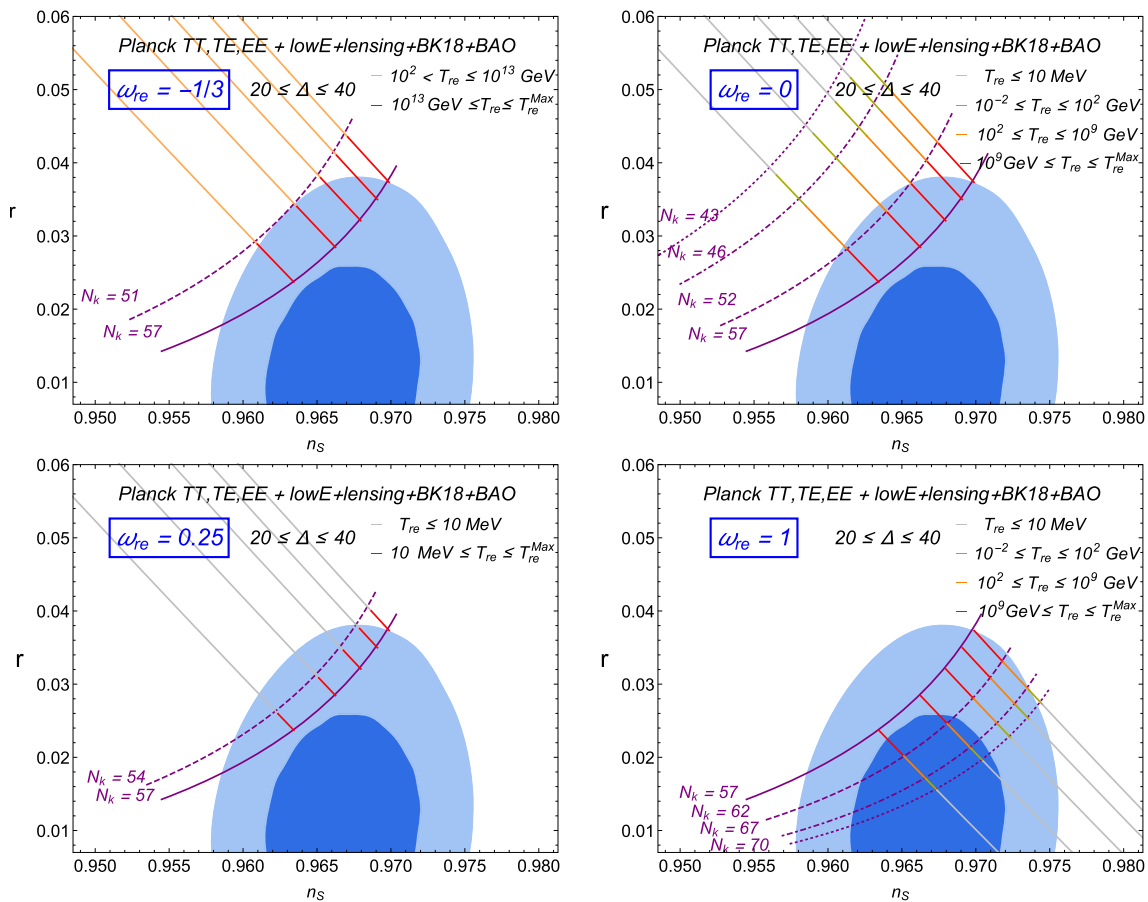
Fig. 4 The $n_S - r$ plot for natural inflation with potential given in Eq. (22). The shaded regions are the same as Fig. 2

where the presence of $\mathcal{A}$ indicates the non-zero effects of the interactions mentioned above. These equations do not depend on details of inflaton potential. To give a sizable effect during inflation, deviating from the standard single-field inflation model in Einstein gravity, the $\mathcal{A}$ should be $\mathcal{A} \gtrsim 1$. Equation (11) shows that the additional interactions in our model significantly enhance the gravitational friction. Consequently, the tensor-to-scalar ratio is suppressed by a factor of $1 + \mathcal{A}$ in Eq. (21). The suppression is more significant if $\mathcal{A} \gg 1$; hence, the inflationary predictions can be compatible with the observations.

In Sect. 3, in light of the latest observational data [10,11, 28], we discussed the theoretical predictions of the natural inflation model with potential given in Eq. (22). Although we have several free parameters, the observable quantities of natural inflation depend only on a single parameter Δ as defined in Eq. (24). In the $n_S - r$ plane in Fig. 2, we showed that the natural inflation model is now compatible with the observational data for a certain parameter range, mainly due to the suppressed tensor-to-scalar ratio r. For the predictions to be consistent with data at 1σ (68% confidence) level, natural inflation is supposed to last slightly longer ($N_k \gtrsim 60$) than usually assumed. The right panel of Fig. 2 shows the

parameter space of M and γ parameters that provides the right value for the amplitude of the CMB spectrum.

Imposing the effective equation-of-state ω_{re} parameter to be constant after inflation, we estimated the duration and the temperature of reheating in terms of inflationary parameters in Eqs. (40) and (41), respectively. In Fig. 3, we plotted Eqs. (40) and (41) as a function of n_S for given Δ and ω_{re} values. The figure shows that the broad ranges of ω_{re} and Δ give compatible results with the CMB predictions on n_S. The combined result with Fig. 4 implies that, if $\omega_{re} > 1/3$, inflation can last long enough – i.e., having $N_* \gtrsim 60$. Thus, it is more compatible with the CMB data, the predictions residing inside the 1σ contour, see Fig. 4 for $\omega_{re} = 1$. For the $\omega_{re} < 1/3$ cases, the maximum number of e-folds in natural inflation is $N_k \simeq 57$; hence the predictions reside inside the 2σ contour only, see Fig. 4 for $\omega_{re} = -1/3$, 0, and 0.25 cases. Our result also shows that the broad range of reheating temperatures, from as low as $\sim \mathcal{O}(10)$ MeV to as large as $\sim \mathcal{O}(10^{15})$ GeV, can be achieved at the end of reheating if the equation of state is closer to $1/3$. The maximum reheating temperature is $T_{re}^{max} \simeq 3 \times 10^{15}$ GeV, corresponding to an instantaneous reheating scenario for which $\omega_{re} = 1/3$ and $N_{re} = 0$.

We conclude that the effects of reheating to inflationary predictions are important to tighten the parameter space of observable quantities, breaking degeneracy between inflationary predictions that otherwise overlap in the $n_S - r$ plane. We also found it is interesting to investigate the phenomenological details of reheating for the $\omega_{re} \gtrsim 1/3$. According to our result, in that case, inflation can last longer than usually assumed; hence more consistent with the CMB data, and the broad range of reheating temperature is also accessible.

Data Availability Statement This manuscript has no associated data or the data will not be deposited. [Authors' comment: This work is a theoretical study; hence, no experimental data has been listed.]

References

1. A.H. Guth, The inflationary universe: a possible solution to the horizon and flatness problems. Phys. Rev. D **23**, 347–356 (1981)
2. A.D. Linde, A new inflationary universe scenario: a possible solution of the horizon, flatness, homogeneity, isotropy and primordial monopole problems. Phys. Lett. B **108**, 389–393 (1982)
3. A.D. Linde, Coleman–Weinberg theory and a new inflationary universe scenario. Phys. Lett. B **114**, 431–435 (1982)
4. A. Albrecht, P.J. Steinhardt, Cosmology for grand unified theories with radiatively induced symmetry breaking. Phys. Rev. Lett. **48**, 1220–1223 (1982)
5. A.D. Linde, Chaotic inflation. Phys. Lett. B **129**, 177–181 (1983)
6. P. de Bernardis et al., [Boomerang], A Flat universe from high resolution maps of the cosmic microwave background radiation. Nature **404**, 955–959 (2000)
7. M. Tegmark et al., [SDSS], Cosmological parameters from SDSS and WMAP. Phys. Rev. D **69**, 103501 (2004)
8. U. Seljak et al., [SDSS], Cosmological parameter analysis including SDSS Ly-alpha forest and galaxy bias: Constraints on the primordial spectrum of fluctuations, neutrino mass, and dark energy. Phys. Rev. D **71**, 103515 (2005)
9. C. Blake, E. Kazin, F. Beutler, T. Davis, D. Parkinson, S. Brough, M. Colless, C. Contreras, W. Couch, S. Croom et al., The WiggleZ Dark Energy Survey: mapping the distance-redshift relation with baryon acoustic oscillations. Mon. Not. R. Astron. Soc. **418**, 1707–1724 (2011)
10. Y. Akrami et al. [Planck], Planck 2018 results. X. Constraints on inflation. Astron. Astrophys. **641**, A10 (2020)
11. P.A.R. Ade et al. [Planck], Planck 2015 results. XX. Constraints on inflation. Astron. Astrophys. **594**, A20 (2016)
12. K. Freese, J.A. Frieman, A.V. Olinto, Natural inflation with pseudo—Nambu–Goldstone bosons. Phys. Rev. Lett. **65**, 3233–3236 (1990)
13. D.H. Lyth, A. Riotto, Particle physics models of inflation and the cosmological density perturbation. Phys. Rep. **314**, 1–146 (1999)
14. J.E. Kim, H.P. Nilles, M. Peloso, Completing natural inflation. JCAP **01**, 005 (2005)
15. F.C. Adams, J.R. Bond, K. Freese, J.A. Frieman, A.V. Olinto, Natural inflation: particle physics models, power law spectra for large scale structure, and constraints from COBE. Phys. Rev. D **47**, 426–455 (1993)
16. K. Freese, W.H. Kinney, On: natural inflation. Phys. Rev. D **70**, 083512 (2004)
17. C. Savage, K. Freese, W.H. Kinney, Natural inflation: status after WMAP 3-year data. Phys. Rev. D **74**, 123511 (2006)
18. K. Freese, W.H. Kinney, Natural inflation: consistency with cosmic microwave background observations of Planck and BICEP2. JCAP **03**, 044 (2015)
19. K. Freese, A coupling of pseudo Nambu–Goldstone bosons to other scalars and role in double field inflation. Phys. Rev. D **50**, 7731–7734 (1994)
20. M. Kawasaki, M. Yamaguchi, T. Yanagida, Natural chaotic inflation in supergravity. Phys. Rev. Lett. **85**, 3572–3575 (2000)
21. N. Arkani-Hamed, H.C. Cheng, P. Creminelli, L. Randall, Extra natural inflation. Phys. Rev. Lett. **90**, 221302 (2003)
22. N. Arkani-Hamed, H.C. Cheng, P. Creminelli, L. Randall, Pseudo-natural inflation. JCAP **07**, 003 (2003)
23. D.E. Kaplan, N.J. Weiner, Little inflatons and gauge inflation. JCAP **02**, 005 (2004)
24. H. Firouzjahi, S.H.H. Tye, Closer towards inflation in string theory. Phys. Lett. B **584**, 147–154 (2004)
25. J.P. Hsu, R. Kallosh, Volume stabilization and the origin of the inflaton shift symmetry in string theory. JHEP **04**, 042 (2004)
26. Q.G. Huang, K. Wang, S. Wang, Inflation model constraints from data released in 2015. Phys. Rev. D **93**(10), 103516 (2016)
27. N.K. Stein, W.H. Kinney, Natural inflation after Planck 2018. arXiv:2106.02089 [astro-ph.CO]
28. P.A.R. Ade et al. [BICEP and Keck], Improved Constraints on Primordial Gravitational Waves using Planck, WMAP, and BICEP/Keck Observations through the 2018 Observing Season. Phys. Rev. Lett. **127**(15), 151301 (2021)
29. J. B. Munoz, Equation-of-state parameter for reheating. Phys. Rev. D **91**(4), 043521 (2015)
30. N. Zhang, Y. B. Wu, J. W.. Lu, C. W. Sun, L. J. Shou, H. Z. Xu, Constraints on the generalized natural inflation after Planck 2018. Chin. Phys. C **44**(9), 095107 (2020)
31. M. Civiletti, B. Delacruz, Natural inflation with natural number of *e*-foldings. Phys. Rev. D **101**(4), 043534 (2020)
32. M. Forconi, W. Giarè, E. Di Valentino, A. Melchiorri, Cosmological constraints on slow roll inflation: an update. Phys. Rev. D **104**(10), 103528 (2021)
33. G. Tumurtushaa, Inflation with derivative self-interaction and coupling to gravity. Eur. Phys. J. C **79**(11), 920 (2019)
34. B. Bayarsaikhan, S. Koh, E. Tsedenbaljir, G. Tumurtushaa, Constraints on dark energy models from the Horndeski theory. JCAP **11**, 057 (2020)
35. P. Chen, S. Koh, G. Tumurtushaa, Primordial black holes and induced gravitational waves from inflation in the Horndeski theory of gravity. arXiv:2107.08638 [gr-qc]

36. T. Kobayashi, M. Yamaguchi, J. Yokoyama, Generalized G-inflation: inflation with the most general second-order field equations. Prog. Theor. Phys. **126**, 511–529 (2011)
37. G.W. Horndeski, Second-order scalar–tensor field equations in a four-dimensional space. Int. J. Theor. Phys. **10**, 363–384 (1974)
38. C. Deffayet, X. Gao, D.A. Steer, G. Zahariade, From k-essence to generalised galileons. Phys. Rev. D **84**, 064039 (2011)
39. M. Ostrogradski, Mem. Ac. St. Petersbourg VI **4**, 385 (1850)
40. T. Kobayashi, Horndeski theory and beyond: a review. Rep. Prog. Phys. **82**(8), 086901 (2019)
41. C. Germani, A. Kehagias, New model of inflation with non-minimal derivative coupling of standard model Higgs boson to gravity. Phys. Rev. Lett. **105**, 011302 (2010)
42. C. Germani, A. Kehagias, UV-protected inflation. Phys. Rev. Lett. **106**, 161302 (2011)
43. S. Tsujikawa, Observational tests of inflation with a field derivative coupling to gravity. Phys. Rev. D **85**, 083518 (2012)
44. S. Tsujikawa, J. Ohashi, S. Kuroyanagi, A. De Felice, Planck constraints on single-field inflation. Phys. Rev. D **88**(2), 023529 (2013)
45. C. Germani, Y. Watanabe, UV-protected (natural) inflation: primordial fluctuations and non-Gaussian features. JCAP **07**, 031 (2011)
46. K. Kamada, T. Kobayashi, M. Yamaguchi, J. Yokoyama, Higgs G-inflation. Phys. Rev. D **83**, 083515 (2011)
47. L.F. Abbott, E. Farhi, M.B. Wise, Particle production in the new inflationary cosmology. Phys. Lett. B **117**, 29 (1982)
48. A.D. Dolgov, A.D. Linde, Baryon asymmetry in inflationary universe. Phys. Lett. B **116**, 329 (1982)
49. A. Albrecht, P.J. Steinhardt, M.S. Turner, F. Wilczek, Reheating an inflationary universe. Phys. Rev. Lett. **48**, 1437 (1982)
50. R. Allahverdi, R. Brandenberger, F.Y. Cyr-Racine, A. Mazumdar, Reheating in inflationary cosmology: theory and applications. Annu. Rev. Nucl. Part. Sci. **60**, 27–51 (2010)
51. S. Dodelson, L. Hui, A horizon ratio bound for inflationary fluctuations. Phys. Rev. Lett. **91**, 131301 (2003)
52. J. Martin, C. Ringeval, First CMB constraints on the inflationary reheating temperature. Phys. Rev. D **82**, 023511 (2010)
53. P. Adshead, R. Easther, J. Pritchard, A. Loeb, Inflation and the scale dependent spectral index: prospects and strategies. JCAP **02**, 021 (2011)
54. J. Mielczarek, Reheating temperature from the CMB. Phys. Rev. D **83**, 023502 (2011)
55. R. Easther, H.V. Peiris, Bayesian analysis of inflation II: model selection and constraints on reheating. Phys. Rev. D **85**, 103533 (2012)
56. L. Dai, M. Kamionkowski, J. Wang, Reheating constraints to inflationary models. Phys. Rev. Lett. **113**, 041302 (2014)
57. P. Creminelli, D. López Nacir, M. Simonović, G. Trevisan, M. Zaldarriaga, ϕ^2 inflation at its endpoint. Phys. Rev. D **90**(8), 083513 (2014)
58. R.G. Cai, Z.K. Guo, S.J. Wang, Reheating phase diagram for single-field slow-roll inflationary models. Phys. Rev. D **92**, 063506 (2015)
59. R.M. Corless, G.H. Gonnet, D.E.G. Hare, D.J. Jeffrey, D.E. Knuth, On the LambertW function. Adv. Comput. Math. **5**, 329–359 (1996)